

SELF-DRIVING AND MODEL-BASED EXTREMUM SEEKING CONTROL IN TIGHT FORMATION FLIGHT FOR FUEL SAVING

Daniel Barbuto Rossato¹ & Karl Heinz Kienitz²

¹Faculdade SENAI São Paulo, email: daniel.rossato@sp.senai.br ²Instituto Tecnológico de Aeronáutica, email: kienitz@ieee.org

Abstract

Fuel consumption in tight formation flight varies according to the position of the follower aircraft within the vortex field generated by the leader aircraft. In this work, three different approaches are analysed for reaching the sweet-spot from an initial position and maintaining proximity to that position in the presence of turbulence, which is described herein using a Dryden model and a one-minus-cosine profile. The first approach fixes a setpoint at a previously computed sweet-spot value. The other two adjust the value "on-the-fly" using real-time optimization algorithms. The second approach resorts to self-driving extremum seeking control, which uses only the value of fuel consumption to determine the setpoint values, but without adding any dither signal. The third approach is a model-based extremum seeking control of the "economic model predictive control" type, which predicts future values to choose the best current setpoint values while considering constraints on those variables.

Keywords: economic model predictive control, extremum seeking control, formation flight, fuel saving

1. Introduction

In the context of tight formation flight aimed at fuel saving, several critical issues must be addressed. Previous studies, such as [1] and [2], discussed the wake vortex model generated by a lead aircraft and its impact on a follower. Initial development of an aircraft autopilot to navigate within, maneuver around, and exit the vortex field was presented in [3], further refined in [4] using a linearized cruise flight model, and in [5] employing a nonlinear model. Flight conditions within the vortex field were analyzed in [6].

The specific challenge addressed here is achieving and maintaining the follower aircraft at the best fuel-saving position, known as the sweet-spot, despite disturbance affecting follower linear velocities. To achieve this, a real-time optimization (RTO) system is required to adjust position setpoints based on relative aircraft coordinates. Fuel consumption serves as the input variable for optimizing setpoint values. Given the unpredictable nature of wind disturbances and their impact on the vortex field and aircraft movements, extremum seeking control (ESC) has been the preferred approach.

Previous studies (e.g., [8], [9], [10], [11], [12]) addressed the sweet-spot problem using traditional ESC algorithms [13], [14], which involve applying a dither signal to induce oscillations in input variables for numerical gradient determination. However, this approach raises concerns regarding comfort, performance, and safety due to oscillations in aircraft variables.

Therefore, in the context of achieving and maintaining the sweet-spot in tight formation flight, a self-driving approach is preferable as it avoids the need for a dither signal to obtain derivative information. This approach aims at smooth aircraft movement within the vortex field, as proposed in algorithms such as [15].

A further real-time optimization (RTO) approach will also be considered herein: economic model predictive control (EMPC). It can be seen as a model-based extremum seeking control, having been studied and applied to chemical engineering problems [16]. MPC methods exist for both linear systems [17] and nonlinear systems [18].

This paper presents the research problem closely integrated with (still initial) practical considerations through a numerical example. Section 2 elaborates on the optimization challenges in tight formation flight for fuel savings, intertwined with the model description of the example used. Section 3 introduces extremum seeking control strategies, while Section 4 focuses on simulations, results, and discussions regarding controller performance. Final considerations are provided in Section 5.

2. Modeling

In this section, the optimization problem is developed. Firstly, the model of the follower aircraft in tight formation flight is presented taking into account disturbances from wind gusts and the wake vortex generated by the leading aircraft. Following this, the model of the closed-loop system is described which includes a multivariable linear controller.

2.1 Follower aircraft

At leveled flight in cruise velocity, the aircraft model can be split in two submodels: lateral and longitudinal. In state-space form, if $I_{xz} = 0$, the lateral motion can be described by the following dynamics:

$$\dot{\mathbf{x}}_{t}(t) = A_{t}\mathbf{x}_{t}(t) + B_{t}\mathbf{u}_{t}(t) + F_{t}\mathbf{d}_{t}(t), \tag{1}$$

where the state variables, inputs variables and the matrices A_t , B_t and F_t are given in equation 2.

$$\begin{bmatrix}
\dot{y}_{o} \\
\dot{v} \\
\dot{p} \\
\dot{r} \\
\dot{\phi} \\
\dot{\psi}
\end{bmatrix} = \underbrace{\begin{bmatrix}
0 & 1 & 0 & 0 & -\bar{w} & \bar{u} \\
0 & Y'_{v} & Y'_{p} + \bar{w} & Y'_{r} - \bar{u} & gc_{\bar{\theta}} & 0 \\
0 & L'_{v} & L'_{p} & L'_{r} & 0 & 0 \\
0 & N'_{v} & N'_{p} & N'_{r} & 0 & 0 \\
0 & 0 & 1 & 0 & 0 & 0 \\
0 & 0 & 0 & 1 & 0 & 0
\end{bmatrix}}_{\mathbf{r}} \underbrace{\begin{bmatrix}
y_{o} \\
v \\
p \\
r \\
\phi \\
\psi
\end{bmatrix}} + \underbrace{\begin{bmatrix}
0 & 0 \\
Y'_{\delta_{a}} & Y'_{\delta_{r}} \\
L'_{\delta_{a}} & L'_{\delta_{r}} \\
N'_{\delta_{a}} & N'_{\delta_{r}} \\
0 & 0 \\
0 & 0
\end{bmatrix}}_{\mathbf{u}_{t}} \underbrace{\begin{bmatrix}
\delta_{a} \\
-L'_{v} & -L'_{p} & -L'_{r} \\
-L'_{v} & -L'_{p} & -L'_{r} \\
-N'_{v} & -N'_{p} & -N'_{r} \\
0 & 0 & 0 \\
0 & 0 & 0
\end{bmatrix}}_{\mathbf{d}_{t}} \underbrace{\begin{bmatrix}
v_{g} \\
p_{g} \\
r_{g}
\end{bmatrix}}_{\mathbf{d}_{t}}$$

$$(2)$$

In that equation, $c_{\bar{\theta}}$ represents $\cos \bar{\theta}$. The variables of the lateral model are defined in Table 1. All variables are considered incremental regarding their trim value.

Table 1 – Variables of the lateral motion

Symbol	State Variable Name	Symbol	Input Variable Name
y_o	lateral position regarding the leading aircraft	δ_a	aileron deflection
v	linear velocity regarding y-axis of the body	δ_r	rudder deflection
p	angular velocity regarding x-axis of the body	v_g	induced velocity in v due to gust
r	angular velocity regarding z-axis of the body	p_g	induced velocity in p due to gust
ϕ	roll angle	r_g	induced velocity in r due to gust
Ψ	vaw angle		

The dynamics of the longitudinal motion is given by the state-space model:

$$\dot{\boldsymbol{x}}_{\boldsymbol{n}}(t) = A_n \boldsymbol{x}_{\boldsymbol{n}}(t) + B_n \boldsymbol{u}_{\boldsymbol{n}}(t) + F_n \boldsymbol{d}_{\boldsymbol{n}}(t), \tag{3}$$

where the state variables, inputs variables and the matrices A_n , B_n and F_n are given in equation 4.

$$\begin{bmatrix} \vec{z}_{o} \\ \vec{x}_{o} \\ \dot{u} \\ \dot{w} \\ \dot{q} \\ \dot{\theta} \\ \dot{\theta}$$

The variables of the lateral model are defined in Table 2. Again, all variables are considered incremental regarding their trim value.

Table 2 – Variables of the longitudinal motion

Symbol	State Variable Name	Symbol	Input Variable Name
$\overline{z_o}$	altitude position regarding the leading aircraft	δ_e	elevator deflection
x_o	longitudinal pos. regarding the leading aircraft	δ_{t}	thrust command
и	linear velocity regarding x-axis of the body	u_g	induced velocity in u due to gust
W	linear velocity regarding z-axis of the body	w_g	induced velocity in w due to gust
q	angular velocity regarding y-axis of the body	q_g	induced velocity in q due to gust
θ	pitch angle		
n_1	engine velocity left(LH) and right(RH)		
$\dot{n_1}$	engine acceleration left(LH) and right(RH)		
ff	engine fuel flow left(LH) and right(RH)		

The values of each derivative and trim values for a twin-engine VFW-ATTAS-614 jet aircraft at a straight-level cruise flight at 6,000 m of altitude and true airspeed of 170 m/s are given in Table 3. State variables that are not described in the table have zero value at the trim condition.

Parameters regarding the propulsion model have the following values: $a_{ff} = 15.92$, $b_{ff} = 148.8$, $a_{1n} = 30.98$, $a_{0n} = 29.45$, $b_{0n} = 4.11$.

2.2 Follower aircraft inside the wake vortex field

The disturbance input is divided into two components. The first component involves the induced velocities arising from the encounter with a wake vortex generated by the leader aircraft. These velocities vary depending on the aircraft's position within the vortex field, specifically along the lateral (y_o) and vertical (z_o) axes. The longitudinal distance x_o is assumed to be constant or subject to minimal

Table 3 – Derivatives and states at trim condition

Force derivatives	Value	Moment derivatives	Value	States at trim	Value
X'_u	-0.011	L_{v}^{\prime}	-0.036	$\bar{u} [m/s]$	169.9
X_w'	0.064	L_p'	-1.506	$\bar{w} [m/s]$	6.908
X_q'	0.023	$\hat{L_r'}$	0.558	$ar{ heta} \ [rad]$	0.041
$X_q' \ Y_v'$	-0.187	M'_u	-0.001	$n_{1_{LH}}^{-} [\%]$	90.63
Y_p'	0.211	M_w'	-0.053	$n_{1_{RH}}^{-}$ [%]	90.63
$Y_p' \ Y_r'$	1.868	M_a'	-1.350	$f\bar{f}_{LH} [g/s]$	230.0
Z_u'	-0.083	N_{v}^{\prime}	0.025	$f\bar{f}_{RH} [g/s]$	230.0
Z_w'	-1.101	N_p'	0.109	$ar{\delta}_{\!tLH} \; [\%]$	41.09
Z_q'	-3.508	N_r'	-0.628	$ar{\delta}_{tRH}~[\%]$	41.09
$X_{n_1}^{''}$	0.016	$L'_{\delta_{\sigma}}$	-8.738	$\bar{z_o}$ [m]	-6000
Y_{δ_a}'	0	$M_{n_1}^{\prime a}$	0.002	_	_
$Z_{n_1}^{a}$	0.003	$N_{\delta_a}^{\prime}$	0.404	_	_
$X_{\delta_e}^{\prime}$	0.114	$L_{\delta_r}^{\prime_a}$	2.297	_	_
Y_{δ_r}'	5.978	$M_{\delta_{e}}^{\prime_{r}}$	-13.04	_	_
$Z_{\delta_e}^{o_r}$	-17.43	N_{δ_r}'	-2.600	_	_

variations, which do not significantly influence the aircraft's velocities. For this analysis, the vortex field is considered to remain constant over time. The second component encompasses the induced velocities due to wind gusts, which alter the vortex field over time. In the equation below, the index v denotes the perturbations caused by the wake vortex and the index w denotes the perturbations resulting from wind gusts.

$$\boldsymbol{d_t}(t) = \boldsymbol{d_{tv}}(y_o, z_o) + \boldsymbol{d_{tw}}(t) \rightarrow \begin{bmatrix} v_g \\ p_g \\ r_g \end{bmatrix} = \begin{bmatrix} v_v(y_o, z_o) \\ p_v(y_o, z_o) \\ r_v(y_o, z_o) \end{bmatrix} + \begin{bmatrix} v_w(t) \\ p_w(t) \\ r_w(t) \end{bmatrix}, \tag{5}$$

$$\boldsymbol{d}_{\boldsymbol{n}}(t) = \boldsymbol{d}_{nv}(y_o, z_o) + \boldsymbol{d}_{nw}(t) \rightarrow \begin{bmatrix} u_g \\ w_g \\ q_g \end{bmatrix} = \begin{bmatrix} u_v(y_o, z_o) \\ w_v(y_o, z_o) \\ q_v(y_o, z_o) \end{bmatrix} + \begin{bmatrix} u_w(t) \\ w_w(t) \\ q_w(t) \end{bmatrix}.$$
 (6)

Data for a discrete static field map along the yo and zo axes were obtained using the Wake Vortex Encounter (WVE) software package. This software, originally developed as part of the European S-Wake project, has been modified to include the model of the wake roll-up in the near field region. The analysis considers a longitudinal distance x_o equivalent to 5 wingspans behind the leader aircraft, where each wingspan measures 21.5 m. Both the follower and leader aircraft are of the same model. Further details can be found in [1] and [3].

Consider the fuel consumption increment within the vortex field depicted in Fig. 1. The optimum point for maximum fuel savings, known as sweet-spot, is identified at coordinates $y_o = 16.5$ and $z_o = 0.0$ [6]. Thus, the region of interest for this work is defined by the boundaries $11 \le y_o \le 25$ and $-5 \le z_o \le 5$ approximately. The optimization loop will be activated only when the aircraft is positioned within this specified region.

2.3 Closed-loop system

A controller for the follower aircraft operating within the wake vortex was developed using a multivariable linear robust control approach. Specifically, the structured H_{∞} algorithm was applied to manage the uncertainties in the model as described in [4]. Figure 2 illustrates the block diagram of the closed-loop system, which includes filters and controllers designed for this purpose. The system incorporates an output-feedback control (K) with a feed-forward gain (K_f) and integral control (K_i) . It also features a setpoint filter (F_s) and a roll-off filter (F_r) to manage the lateral (t) and longitudinal

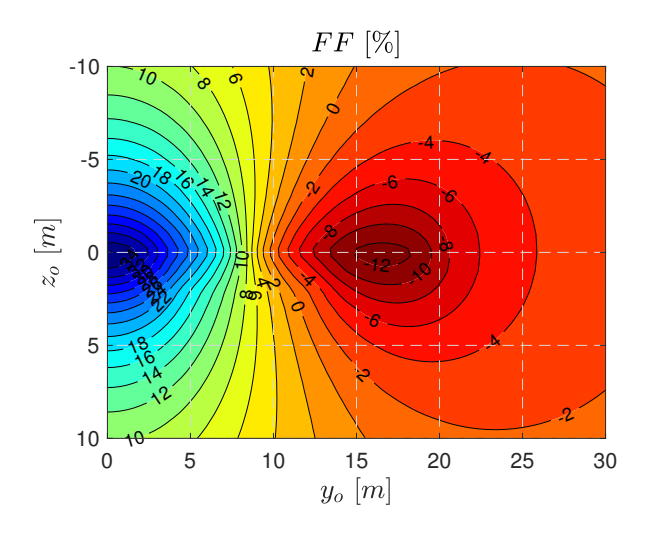


Figure 1 – Fuel consumption increment inside the vortex field.

(n) dynamics. The blocks labeled C, E and H represent matrices that are used to extract the output variables from the state variables.

The gains of the output-feedback matrices are:

$$K_{t} = \begin{bmatrix} -0.15 & 7.90 & -0.08 & -27.73 & 2.47 & -58.31 \\ 0.21 & 2.75 & 1.16 & -30.68 & 1.47 & 19.92 \end{bmatrix}$$

$$K_{n} = \begin{bmatrix} 0.18 & -0.05 & 0.03 & 0.13 & -1.87 & -24.94 \\ -1.15 & 3.6 & 16.64 & 1.04 & 51.33 & -54.34 \end{bmatrix}.$$

$$(7)$$

The feed-forward gains are:

$$K_{ft} = \begin{bmatrix} -0.15 \\ 0.21 \end{bmatrix}, \quad K_{fn} = \begin{bmatrix} 0.18 & -0.05 \\ -1.15 & 3.6 \end{bmatrix}.$$
 (8)

The integral control matrices are:

$$K_{it} = \begin{bmatrix} -0.1/s \\ 0.2/s \end{bmatrix}, \quad K_{in} = \begin{bmatrix} 0.24/s & -0.01/s \\ -0.57/s & 0.33/s \end{bmatrix}.$$
 (9)

The setpoint filters are given by:

$$F_{st} = \begin{bmatrix} \frac{1}{4s^2 + 4s + 1} \end{bmatrix}, \quad F_{sn} = \begin{bmatrix} \frac{1}{s^2 + 2s + 1} & 0\\ 0 & \frac{1}{4s^2 + 4s + 1} \end{bmatrix}. \tag{10}$$

And the roll-off filters are given by:

$$F_{rt} = \begin{bmatrix} \frac{1}{0.35s+1} & 0\\ 0 & \frac{1}{0.35s+1} \end{bmatrix}, \quad F_{rn} = \begin{bmatrix} \frac{1}{0.35s+1} & 0\\ 0 & \frac{1}{0.51s+1} \end{bmatrix}.$$
 (11)

The output matrices are:

$$C_t = I_6, \quad C_n = \begin{bmatrix} I_6 & \theta_{6 \times 6} \end{bmatrix}, \quad H_n = \begin{bmatrix} \theta_{1 \times 8} & 1 & 0 & 0 & 1 \end{bmatrix}.$$
 (12)

The wingman aircraft model is composed of lateral (Eq. 2) and longitudinal models (Eq. 4).

3. Extremum seeking control

This section outlines the optimization problem and provides a brief explanation of the algorithms for extremum seeking control: self-driving and economic model predictive control.

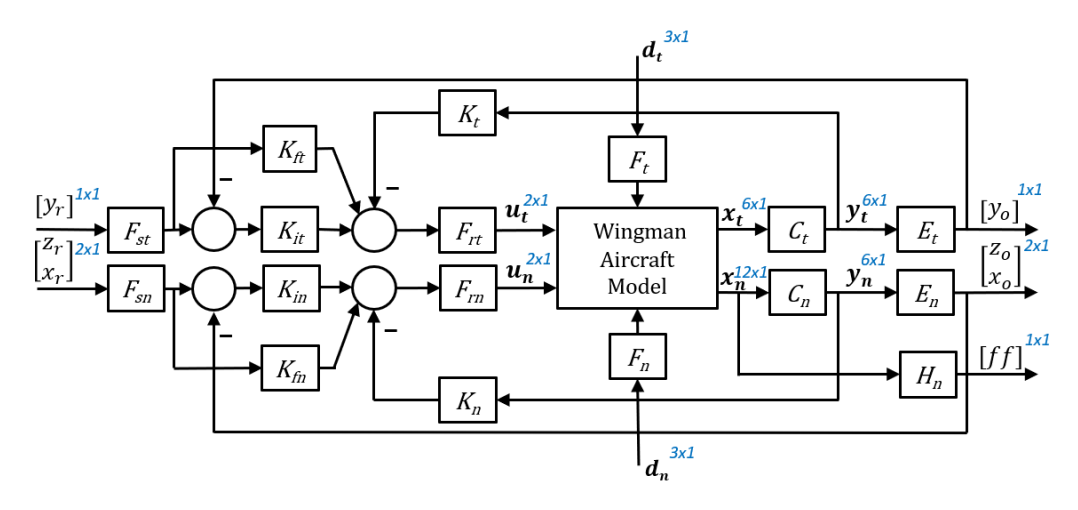


Figure 2 – Closed-loop block diagram.

3.1 The problem model

The problem model is summarized as depicted in Fig. 3. In this diagram, G_{cl} represents the equivalent linear model of the closed-loop system. The lookup table functions as a static, nonlinear mapping from the relative coordinates (y_o and z_o) to the induced velocities in the lateral and longitudinal directions caused by the wake vortex..

The challenge addressed here is how to adjust the setpoint values of the relative position $(y_r \text{ and } z_r)$ of the aircraft within the vortex field to minimize the output fuel flow (ff), accounting for gusts $(d_t \text{ and } d_n)$ originating from both the wake vortex of the leader aircraft and environmental disturbances.

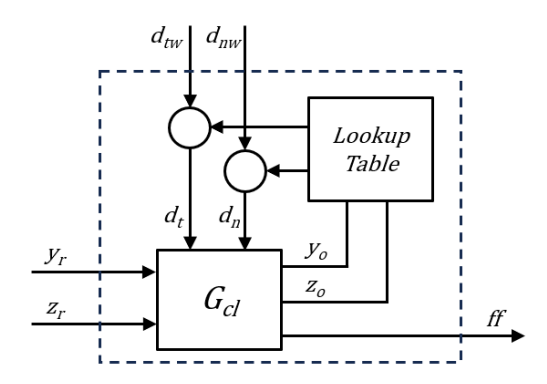


Figure 3 – The problem model.

There are essentially three approaches to solving this problem. The first method involves maintaining the aircraft at the known sweet spot coordinates. However, if the vortex field changes due to movements of the leader aircraft, such changes must be detected and the new sweet spot coordinates computed accordingly. An example of this control strategy, which considers a turn in the leader aircraft's trajectory, is discussed in [2]. This approach utilizes bank angle adjustments to accurately recalibrate the wake vortex's influence relative to the current aircraft coordinates.

The second approach treats the system as a black-box and employs an optimization algorithm to dynamically locate the sweet-spot. This adaptive control method focuses on optimizing steady-state performance in real-time, known as extremum seeking control (ESC).

Formally, the problem can be defined using an objective function that expresses the steady-state relationship between the setpoint signal (or parameters of a feedback law) and the energy expenditure (or another performance variable). The extremum (minimum or maximum) of that function corresponds to the optimal steady-state performance [7].

Consider a nonlinear plant:

$$\dot{x}(t) = f(x(t), u(t))
y(t) = h(x(t), u(t)),$$
(13)

where x is the state vector, the input u is a tunable parameter (in this case, the setpoint of the relative coordinates y_r and z_r) and the output y is a measure for the performance (in this case, fuel consumption f(f)).

Consider the objective function be y = F(u). In this context, suppose that the lowest (highest) steady-state value of y represents a unique minimum (maximum) of the objective function, indicating optimal plant performance. This unique value is defined (in the case of a minimum) by:

$$u^* = \underset{u \in \mathbb{R}}{\arg \min} \ F(u). \tag{14}$$

An ESC algorithm aims to converge the input u towards u^* , typically focusing on local optimization in practice. Various approaches have been developed for this purpose, many of which are derivative-based optimization methods. These methods involve computing or estimating the gradient of the objective function to determine an update direction for u that achieves convergence to u^* . A conventional approach involves the introducing a perturbation signal (dither) into the variables to induce oscillations and facilitate gradient determination.

The third solution involves modeling the system, thus it is considered a white-box approach. This approach uses the system model to predict the values of variables in the near future (prediction horizon). Model predictive control aims to select the best next value of the input system that minimize a cost function, taken into account the plant dynamics and constraints regarding input and output variables. Control actions are updated as new observations become available through feedback. The controller typically operates at discrete time intervals, and the optimization task is repeated each sampling time [17].

3.2 Self-driving extremum seeking control

A self-driving extremum seeking control scheme (SD-ESC) was proposed in [15] and is illustrated in Fig. 4.

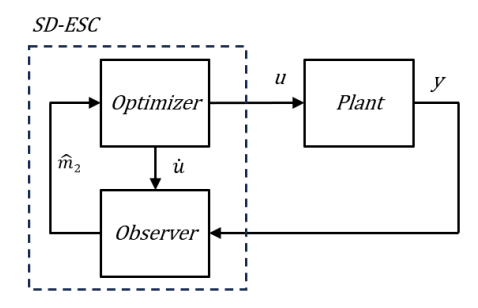


Figure 4 – Self-driving extremum seeking control

The observer estimates the gradient of the objective function based on the measurement of the plant output y and the derivative of the signal u applied to the plant. The output of the observer is denoted as the estimated gradient $\hat{m_2}$. The observer comprises four states: $\hat{m_1}$, $\hat{m_2}$, Q_1 and Q_2 whose initial values must be chosen appropriately. These states are computed as follows:

$$\dot{\hat{m}}_{1}(t) = \eta (y(t) - \hat{m}_{1}(t))
\dot{\hat{m}}_{2}(t) = \eta Q_{2}(t)Q_{1}(t)(y(t) - \hat{m}_{1}(t) - Q_{1}(t)\hat{m}_{2}(t))
\dot{Q}_{1}(t) = -\eta Q_{1}(t) + \dot{u}(t)
\dot{Q}_{2}(t) = \eta Q_{2}(t) - \eta Q_{1}^{2}(t)Q_{2}^{2}(t)$$
(15)

The optimizer utilizes the estimated gradient to calculate the signal u according to the direction of gradient descent. The parameter λ adjust the size of each descent step.

$$\dot{u}(t) = -\lambda \, \eta \, \hat{m}_2(t) \tag{16}$$

The state variable $\hat{m_1}$ estimates \dot{y} using the measured signal y as the input of a first-order transient attenuation filter with time constant η . The parameter η is tuned to account for plant dynamics and the expected convergence rate. State variable Q_1 filters the output signal \dot{u} from optimizer block using a first-order filter with time constant η . State variable $\hat{m_2}$ estimates \dot{u} using the other states to approximate the ratio of the filtered signals \dot{y} and \dot{u} .

The dynamics of the state variable Q_2 addresses the challenge of computing the gradient estimated by $\hat{m_2}$, where Q_2 is inversely proportional to Q_1^2 . As the algorithm's output signal u approaches the optimal value u^* , Q_2 increases, potentially causing instability near the optimal value. Additionally, Q_2 acts as an amplification factor for measurement noise. To maintain numerical stability and mitigate the effect of measurement noise, a regularization term $(\sigma > 0)$ is introduced in the equations to constrain Q_2 [19],[15]:

$$\dot{\hat{m}}_{2}(t) = \eta Q_{2}(t)Q_{1}(t)\left(y(t) - \hat{m}_{1}(t) - Q_{1}(t)\hat{m}_{2}(t)\right) - \sigma \eta Q_{2}(t)\hat{m}_{2}(t)
\dot{Q}_{2}(t) = \eta Q_{2}(t) - \eta Q_{1}^{2}(t)Q_{2}^{2}(t) - \sigma \eta Q_{2}^{2}(t).$$
(17)

Neverthless, introducing a regularization term prevents exact convergence to the optimal value u^* . A smaller σ implies a smaller distance $|u-u^*|$. To achieve rapid convergence, select higher values for the tuning parameters λ and η . However, excessively high values can lead to instability in the extremum seeking scheme.

3.3 Economic model predictive control (EMPC)

Economic Model Predictive Control is a control strategy that optimizes economic objectives, such as cost or profit, instead of performance metrics like tracking error or stability used in conventional MPC. It utilizes a plant model to predict future values, incorporating constraints on the cost function to analyze limitations on input and state variables. [23]

Let N denote the Prediction Horizon, representing the number of future time steps over which the system's behavior is predicted, and M the Control Horizon, the number of future time steps over which control actions are optimized ($M \le N$). The EMPC problem is formulated as a constrained optimization problem at discrete time, aiming to determine the optimal control sequence $u(k), u(k+1), \ldots, u(k+M-1)$ that minimizes economic costs over the prediction horizon, subject to system dynamics and constraints [18] [22]:

$$\min_{u} J = \sum_{i=0}^{N-1} L(x(k+i), u(k+i)) + F(x(k+N))$$
s.t. $x(k+i+1) = f(x(k+i), u(k+i)), i = 0, ..., N-1$

$$x(k) = x_{k}$$

$$u_{min} \le u(k+i) \le u_{max}$$

$$du_{min} \le \Delta u(k+i) / \Delta t \le du_{max}$$

$$x_{min} \le x(k+i) \le x_{max}$$

$$dx_{min} \le \Delta x(k+i) / \Delta t \le dx_{max}$$
(18)

where Δt denotes the sampling time, k represents the current time step, x_k denotes the estimated state of the plant observed by the EMPC algorithm, f(x,u) refers to the prediction model that describe the system's state transitions based on the control inputs, L(x,u) is the cost function assessing economic performance at each time step, and F(x) is the terminal cost function evaluating economic performance at the end of the prediction horizon. For $i \geq M$, the control u remains constant at u(k+M-1).

The algorithm reads the current state values x_k and solves the optimization problem at each time step k to determine the optimal control sequence $u(k), u(k+1), \ldots, u(k+M-1)$. Subsequently, it applies the first control action u(k) to the system. At the next time step k+1, it updates the state x(k+1) based on the applied control and repeats the optimization process with the updated state.

4. Simulation and results

In this section, the results of the simulation of three approaches are presented: maintaining a fixed setpoint at the known sweet-spot position, employing self-driving extremum seeking control (SD-ESC) - in fact, two SD-ESC approaches (one for each reference signal) as depicted in Fig.5, - and utilizing economic model predictive control (EMPC).

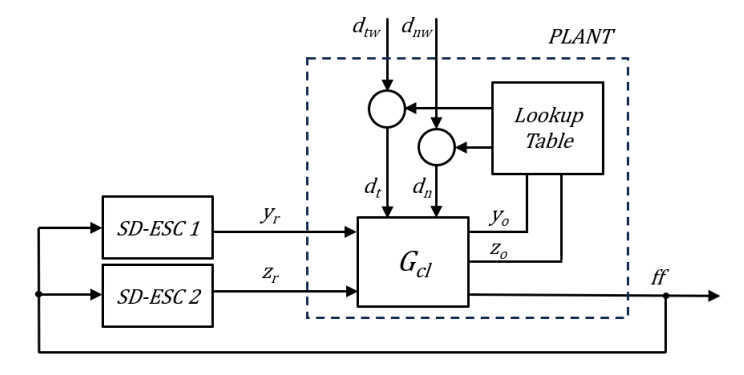


Figure 5 – Self-driving extremum seeking control applied

The SD-ESC algorithms were adapted to a gain scheduling scheme at λ and σ to achieve rapid convergence from initial values and slow convergence near the sweet-spot. This adjustment is motivated by the behavior depicted in Fig. 7, where the surface exhibits a nonsmooth function at z_o axis and the gradient increases in magnitude near the sweet-spot ($z_o = 0$).

After some trial-and-errors, the parameter values chosen for the SD-ESC 1 were:

$$\lambda_{min} = 0.06, \ \lambda_{max} = 10, \ \sigma_{max} = 10^{-4}, \ \sigma_{min} = 10^{-7}, \ \eta = 0.05, \ \text{dir} = 1$$
 (19)

The parameters values chosen for the SD-ESC 2 were:

$$\lambda_{min} = 0.03, \ \lambda_{max} = 6, \ \sigma_{max} = 10^{-3}, \ \sigma_{min} = 10^{-6}, \ \eta = 0.06, \ \text{dir} = -1$$
 (20)

Fig. 6 depicts the application of the EMPC algorithm. The no-measured states of the plant are estimated by an observer scheme (Kalman Filter) based on the inputs and measured states.

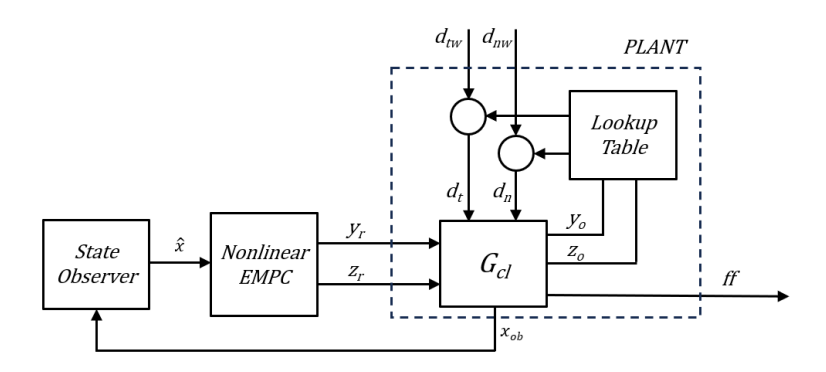


Figure 6 – Economic model predictive control applied

The prediction model was derived from the equivalent closed-loop model (Fig. 2 and the lookup table of induced velocities from the wake vortex. The cost function calculates the aircraft's fuel consumption within the vortex field using a lookup table illustrated in Fig. 1 and depicted in detail in the mesh

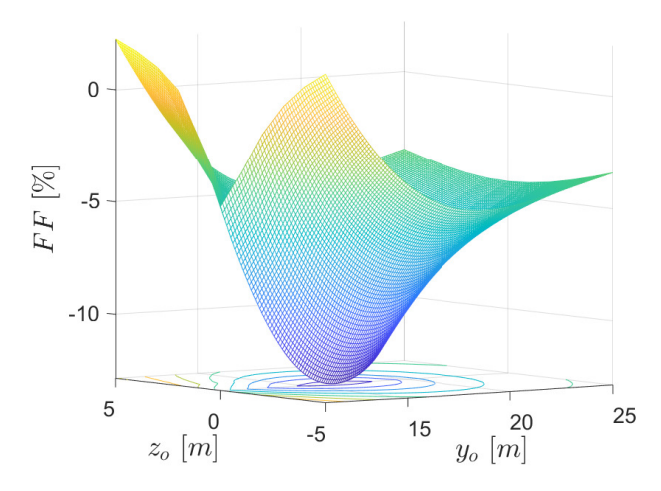


Figure 7 – Fuel consumption increment inside the vortex field

graph of Fig. 7. Specifically, cost function value is determined as the mean fuel consumption over the prediction horizon.

Restrictions were configured to the input and output signals as follows:

$$y_{r_{min}} = 5, \ y_{r_{max}} = 30, \ z_{r_{min}} = -15, \ z_{r_{max}} = 15, (\Delta y_r/\Delta t)_{min} = -5, \ (\Delta y_r/\Delta t)_{max} = 5, \ (\Delta z_r/\Delta t)_{min} = -5, \ (\Delta z_r/\Delta t)_{max} = 5.$$
(21)

where sampling time Δt in this case is 8 seconds. The prediction horizon (N) was set to 6, and the control horizon (M) to 1. These parameter values were selected based on the principles outlined in [20] and [21], considering the plant's step response. The control horizon, when multiplied by the sampling time, is chosen to approximate the settling time of the plant. A low control horizon value ensures robustness against noise and rapid disturbances.

4.1 Case 1: approaching to the sweet spot

Two scenarios involving the search for the sweet-spot were analyzed through simulations conducted in the Simulink environment. The first scenario aimed to find the sweet-spot starting from the initial point $y_r = y_o = 21.0$ and $z_r = z_o = -5.0$.

The graphs in Fig. 8 show the behaviour of the relative coordinates y_o and z_o alongside their respective setpoint (or reference) variables y_r and z_r indicated by dashed lines. For the fixed setpoints (FS), the reference value transitions from the initial point to the sweet-spot within 5 seconds to allow the control system sufficient time to stabilize the aircraft (Figs. 8 a and b). The response is rapid, reaching the final value in approximately 16 seconds.

Using the SD-ESC algorithm (Figs. 8 c and d), the aircraft reaches its final position in two steps over 250 seconds. The initial step achieves rapid progress due to high gains. However, in the subsequent step with reduced gains, the aircraft approaches the vicinity of the sweet-spot more cautiously to avoid instability stemming from the nonsmooth function at z_o . An additional challenge arises from controlling a single variable ff with two inputs $(y_r$ and $z_r)$, each employing its own ESC algorithm. This necessitates simultaneous adjustment of the gains of both ESCs to synchronize their impact on the behavior of the variables y_o and z_o affecting ff.

In Figs. 8 e and f, the EMPC algorithm also swiftly converges towards a position near the sweet-spot. Sequential Quadratic Programming (SQP) was employed to iteratively solve the constrained nonlinear optimization problem. However, like SD-ESC, EMPC faces challenge in achieving an optimal solution when dealing with nonsmooth objective functions.

Fig. 9 d illustrates the trajectory of the aircraft within the vortex field for each strategy utilized, with the sweet-spot denoted by an "x" symbol. Both SD-ESC and EMPC halt in the vicinity of the sweet-spot due to aforementioned reasons, primarily the challenge posed by descent profile and nonsmoothness in the objective function along the z_o direction, as well as the complexity of managing two inputs (y_r and z_r) to control a single output (ff). SD-ESC reaches a final position of $y_o = 16.2$ and $z_o = 0.1$ achieving a fuel economy of 12.5%. EMPC ends at $y_o = 16.6$, $z_r = 0.3$ yielding a fuel economy of 12.8% (compared to a maximum of 12.9% at the sweet spot $y_r = 16.5, z_r = 0$).

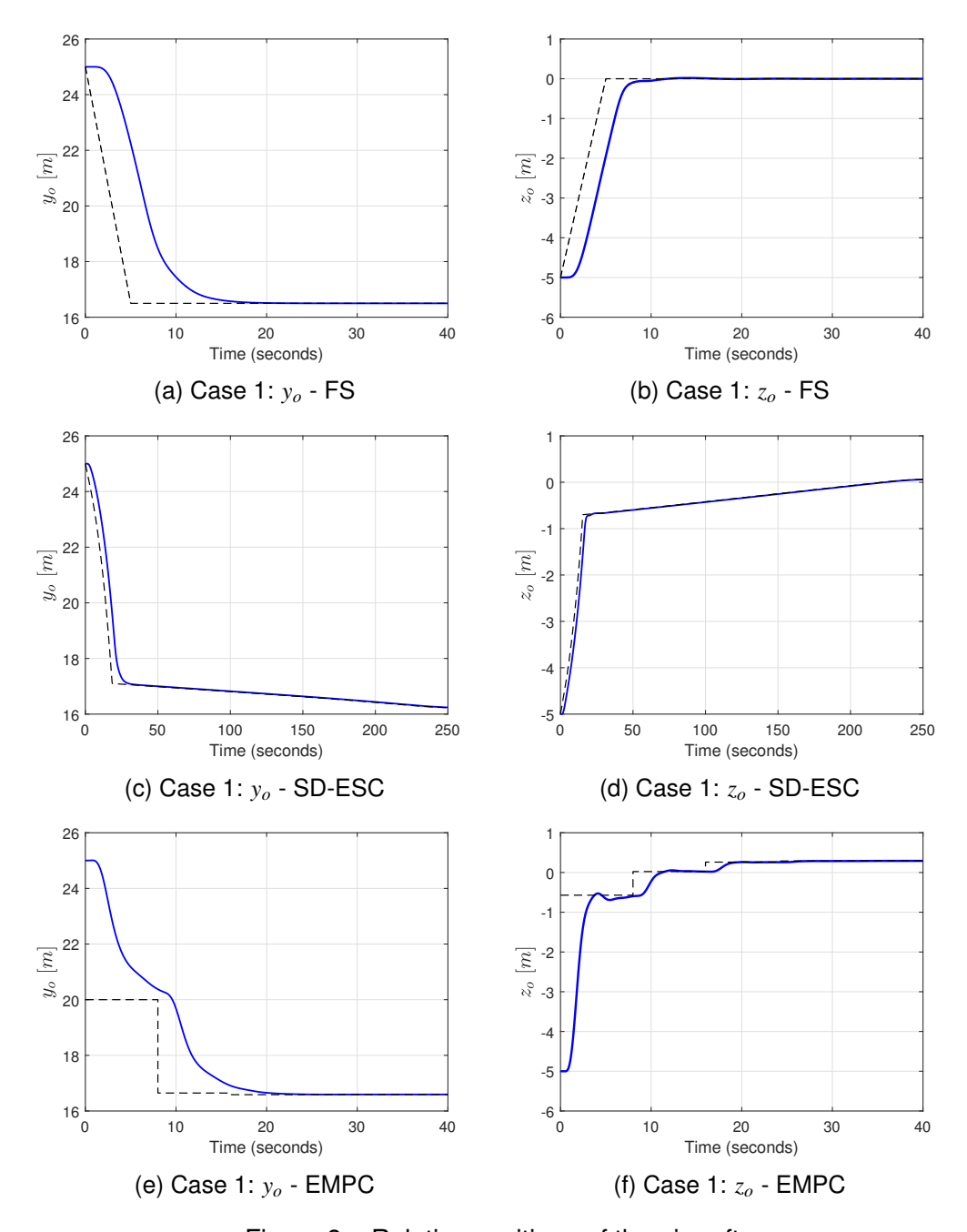


Figure 8 - Relative positions of the aircraft

Concerning the attitude angles in Fig. 9, it is noteworthy that the EMPC strategy resulted in reducing oscillation in ϕ , ψ and θ . This outcome can be attributed to the constraints on the rate of change in setpoint signals implemented within the optimization algorithm, as well as the chosen sampling time. A lower sampling time and a longer control horizon tend to induce greater oscillatory behavior in the aicraft.

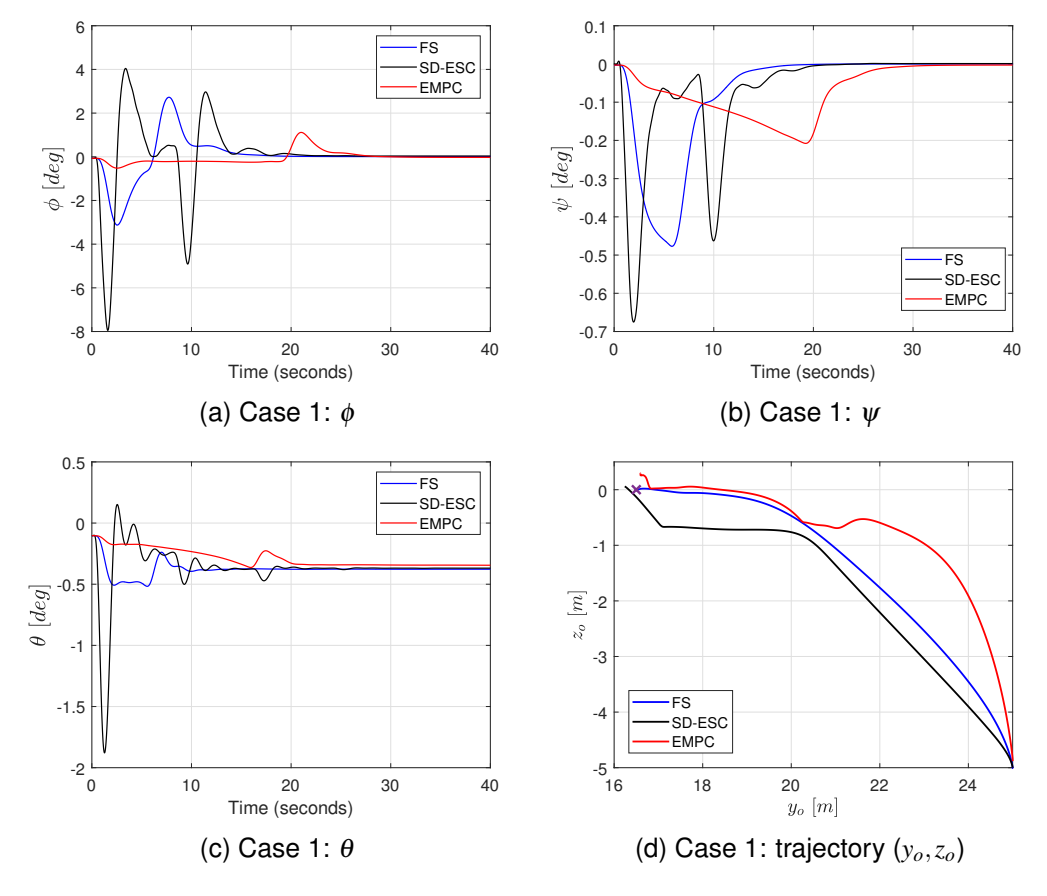


Figure 9 – Aircraft attitude and trajectory

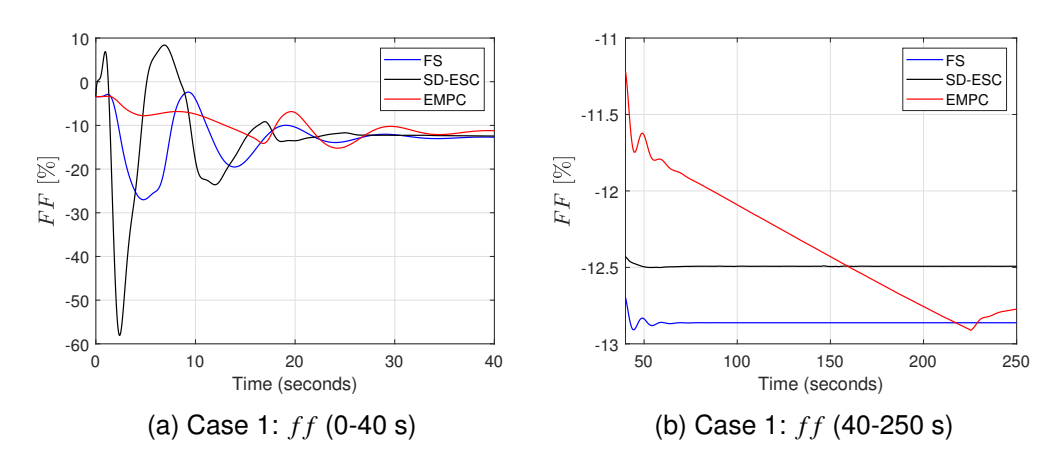


Figure 10 - Fuel consumption

4.2 Case 2: maintaining position despite turbulence

In this scenario, the objective is to maintain the aircraft's position at the sweet-spot despite turbulence, modeled using the one-minus-cosine profile and Dryden turbulence model according to MIL-F-8785-C specification. Turbulence conditions are simulated starting at 250 seconds, lasting 100 seconds in $u_w(t)$, $v_w(t)$ and $w_w(t)$ governed by a continuous Dryden model suitable for high altitudes (scale length = 533.4), sampled every 0.1 seconds with a 0.1 probability of high altitude intensity. At 350 seconds, this turbulence ceases, followed by a new turbulence onset at 400 seconds, also affecting $u_w(t)$, $v_w(t)$ and $w_w(t)$ but utilizing a one-minus-cosine model with an amplitude of 0.1 and a length of 200 meters.

The graphs in Fig. 11 demonstrate that the SD-ESC algorithm exhibits greater variation due to its approach of optimizing based on current values of y_o and z_o whereas EMPC calculates future values

using a prediction model, with the objective function averaging these values over time. This distinction in variability is also evident in Fig. 12.

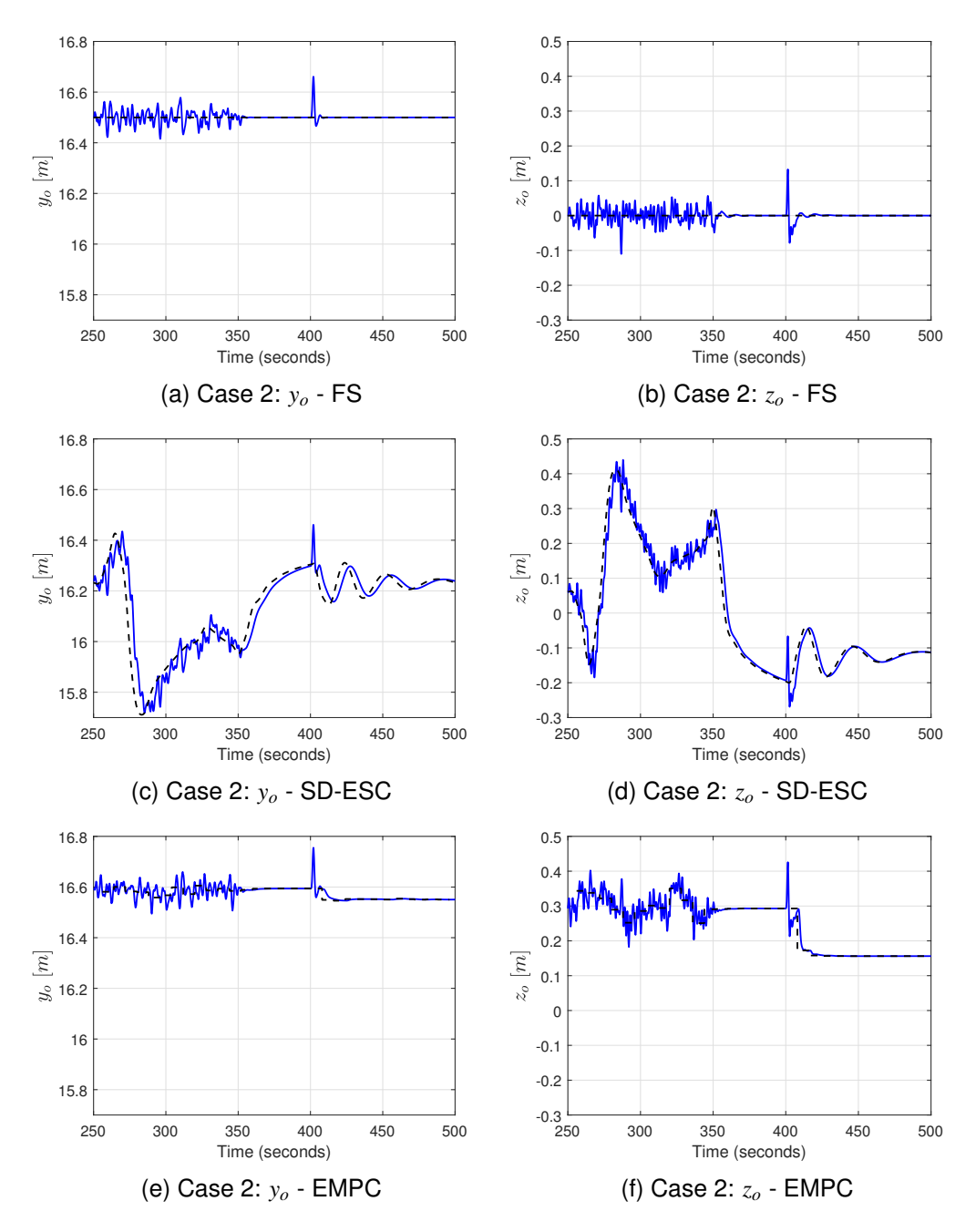


Figure 11 – Relative positions of the aircraft

5. Final considerations

Three approaches were applied to maximize fuel savings in tight formation flight. Initially, a fixed setpoint was chosen based on a pre-computed sweet-spot value. The other two approaches utilized real-time optimization (RTO). The second approach, a black-box self-driving method (SD-ESC), adjusted setpoint variables using current fuel consumption data for optimization. The third approach, a white-box or model-based method called economic model predictive control (EMPC), utilized current state information, a prediction model, and an objective function to compute optimal setpoint values through an optimization algorithm.

This study assessed the performance of each approach under two scenarios: seeking the sweet-spot from an initial position within the vortex field and maintaining position near the sweet-spot despite tur-

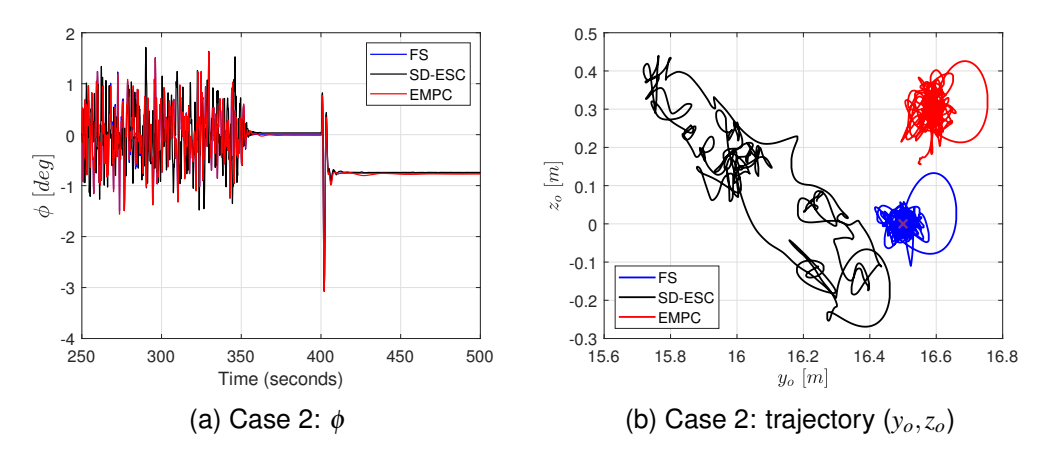


Figure 12 - Aircraft attitude and trajectory

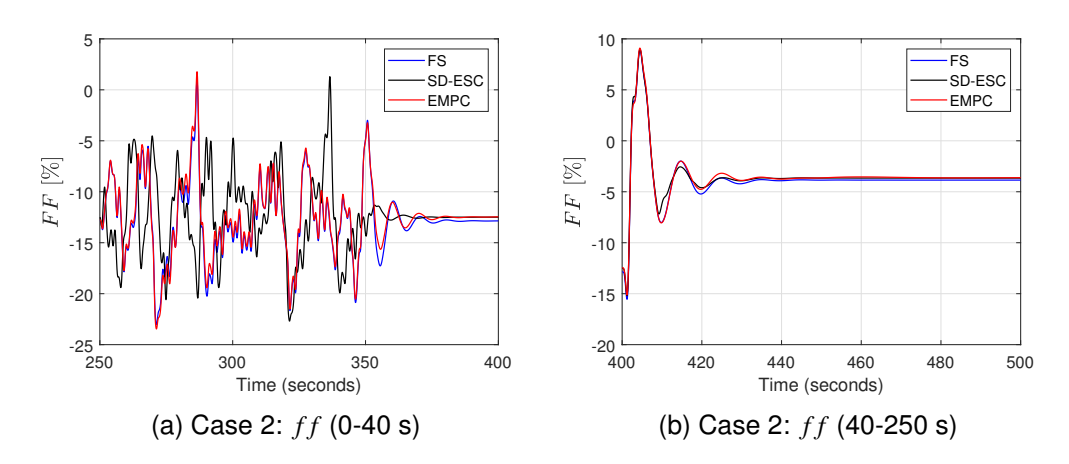


Figure 13 – Fuel consumption

bulence simulated by the Dryden model and one-minus-cosine profile. Each approach demonstrated distinct advantages and disadvantages.

The fixed setpoint approach proved robust in turbulent conditions since it does not require continuous optimization, thereby minimizing aircraft variations.

SD-ESC exhibited high sensitivity to turbulence and might need to be disabled for safety and comfort reasons under such conditions. However, it could be beneficial when the relative coordinates of the sweet-spot change due to maneuvers by the leader aircraft, although it requires improvements to handle nonsmooth functions and dual input variables simultaneously.

Constraints on variables are configurable within EMPC and play a crucial role in preventing aircraft from entering unstable regions within the vortex field, while also limiting the rate of change in setpoint variables to reduce oscillations. Moreover, EMPC operates as a discrete-time algorithm, making it well-suited for handling discrete signals from aircraft positioning systems like GNSS. However, addressing nonsmooth functions in the objective function remains a significant challenge that requires the development of optimization algorithms. Additionally, deploying the algorithm within an aircraft controller necessitates further investigation into real-time computing capabilities.

Future research should investigate the behavior of these algorithms during leader aircraft maneuvers, explore enhanced versions or combined strategies to improve performance, and address the challenge of deploying these algorithms in real-time aircraft controllers.

6. Contact author email address

For more information, contact the first author at daniel.rossato@sp.senai.br

7. Copyright statement

The authors confirm that they, and/or their company or organization, hold copyright on all of the original material included in this paper. The authors also confirm that they have obtained permission, from the copyright holder of any third party material included in this paper, to publish it as part of their paper. The authors confirm that they give permission, or have obtained permission from the copyright holder of this paper, for the publication and distribution of this paper as part of the ICAS proceedings or as individual off-prints from the proceedings.

8. Acknowledgment

The first author acknowledges support of the SENAI-SP Research Group in Electric Engineering, Electronics, Automation and Re-industrialization. The second author acknowledges partial support through grant #304557/2021-8 from CNPq, Brazil.

References

- [1] Kaden A and Luckner R. Modeling wake vortex roll-up and vortex-induced forces and moments for tight formation flight. *AIAA Modeling and Simulation Technologies (MST) Conference*, Boston, MA, 2013. doi: 10.2514/6.2013-5076
- [2] Kaden A and Luckner R. Maneuvers during automatic formation flight of transport aircraft for fuel savings. *Journal of Aircraft*, Vol. 59, No. 2, pp 433-446, 2022. doi: 10.2514/1.C036339
- [3] Kienitz K H, Kaden A and Luckner, R. Modeling and design considerations for robust control of aircraft in tight cruise formation. *AIAA Guidance, Navigation and Control (GNC) Conference*, Boston, MA, 2013. doi: 10.2514/6.2013-4858
- [4] Rossato D B and Kienitz K H. Structured H_{∞} synthesis: a systematic design approach for fully and underactuated systems. *Aerospace and Science Technology (AESCTE)*, Vol. 119, 2021. doi: 10.1016/j.ast.2021.107171
- [5] Niestroy M, Luckner R and Doll C. Flight control systems for aircraft engaged in air wake surfing for efficiency. *AIAA Scitech 2020 Forum*, Orlando, FL, 2020. doi: 10.2514/6.2020-1003
- [6] Rossato D B and Kienitz K H. Conditions of flight of wingman aircraft in tight formation flight for fuel saving. 33rd Congress of the International Council of the Aeronautical Sciences (ICAS), Stockholm, ICAS, 2022.
- [7] Haghi P. ES-MRAC: a new paradigm for adaptive control. PhD thesis, Purdue University, 2014.
- [8] Binetti P, Ariyur K, Krstic M and Bernelli F. Formation flight optimization using extremum seeking feedback. *AIAA Journal of Guidance, Control and Dynamics*, Vol. 26, No. 1, pp 132–142, 2003. doi: 10.2514/2.5024
- [9] Ryan J J and Speyer J L. Peak-seeking control using gradient and hessian estimates. *American Control Conference*, Baltimore, MD, 2010. doi: 10.1109/ACC.2010.5531081
- [10] Hanson C and Ryan J. Peak-seeking optimization of spanwise lift distribution for wings in formation flight. AIAA Guidance, Navigation and Control (GNC) Conference, Minneapolis, MN, 2012. doi: 10.2514/6.2012-4692
- [11] Brown N and Schaefer J. Peak-seeking optimization of trim for reduced fuel consumption: flight test results. *AIAA Guidance, Navigation and Control (GNC) Conference*, Boston, MA, 2013. doi: 10.2514/6.2013-5171
- [12] Brodecki M and Subbarao K. Autonomous formation flight control system using in-flight sweet-spot estimation. *AIAA Journal of Guidance, Control and Dynamics*, Vol. 38, pp 1–14, 2014. doi: 10.2514/1.G000220
- [13] Krstič M and Wang H H. Stability of extremum seeking feedback for general nonlinear dynamic systems. *Automatica*, Vol. 36, No. 4, pp 595–601, 2000. doi: 10.1016/S0005-1098(99)00183-1
- [14] Ariyur K and Krstic M. Real-time optimization by extremum seeking control. Wiley, 2003.
- [15] Haring M A. Extremum-seeking control: convergence improvements and asymptotic stability. PhD thesis, Norwegian University of Science and Technology, 2016.
- [16] Seborg D E, Edgar T F, Mellichamp D A and Doyle F J. *Process dynamics and control.* 4th edition, Wiley, 2016.
- [17] Maciejowski J M. Predictive control with constraints. Prentice-Hall, 2002.

- [18] Grüne L and Pannek J. *Nonlinear model predictive control: theory and algorithms*. 2nd edition, Springer, 2017.
- [19] Guay M and Dochain D. A time-varying extremum-seeking control approach. *Automatica*, Vol. 51, pp 356–363, 2015. doi: 10.1016/j.automatica.2014.10.078
- [20] Shridhar, R and Cooper, D J. A tuning strategy for unconstrained SISO model predictive control. *Industrial and Engineering Chemistry Research*, Vol. 36, No. 3, pp 729-746, 1997.
- [21] Dougherty, D and Cooper, D J. Tuning guidelines of a dynamic matrix controller for integrating non-self-regulating processes. *Industrial & Engineering Chemistry Research*, Vol. 42, No. 8, pp 1739-1752, 2003. doi: 10.1021/ie020546p
- [22] Tran, T and Linga, K-V and Maciejowski, J M. Economic model predictive control a review. *31st International Symposium on Automation and Robotics in Construction*, Sydney, AU, 2014. doi: 10.22260/IS-ARC2014/0006
- [23] Rawlings, J B and Angeli D and Bates C N. Fundamentals of economic model predictive control. *51st IEEE Conference on Decision and Control (CDC)*, Maui, HI, USA, 2012. doi: 10.1109/CDC.2012.6425822